CERN-TH.6247/91

DISCOVERY LIMIT OF THE CHARGED HIGGS BOSON VIA TOP QUARK DECAY AT FUTURE HADRON COLLIDERS

D.P. Roy[*)]

Theoretical Physics Division, CERN
CH-1211 Geneva 23

ABSTRACT

We study the kinematic cuts which can be used to enhance the charged Higgs signal over the W boson background, for $m_{H^\pm} > m_W$, in the decay of a heavy top quark at LHC energy. With suitable cuts it is possible to ensure a sizeable signal and a signal-to-background ratio $\gtrsim 1$ up to $m_{H^\pm} \simeq m_t$ - 20 GeV, which hold throughout the allowed coupling parameter $(tan\beta)$ space in the minimal SUSY model. Thus one should be able to search for the charged Higgs boson to within 20 GeV of the parent top quark mass at the LHC/SSC colliders, i.e., up to 130 GeV for $m_t \simeq 150$ GeV, going up to 180 GeV for $m_t \simeq 200$ GeV.

---

*) On sabbatical leave from the Tata Institute of Fundamental Research, Bombay, 400005, India.

CERN-TH.6247/91
October 1991

The results of the top search experiment at the Tevatron $\bar{p}p$ collider [1] as well as the $B_d - \bar{B}_d$ mixing data [2] suggest a heavy top quark of mass $m_t > 80$ GeV. Moreover, the radiative correction to the W, Z masses suggests a central value of top quark mass $m_t \simeq 150$ GeV with an upper bound of about 200 GeV [3]. A top quark in this mass range is expected to be seen at the Tevatron upgrade and produced more copiously at the LHC/SSC colliders [4]. Besides providing direct evidence for top, this will enable one to search for new particles in the top quark decay; the large top quark mass offers the possibility of carrying on the search to a hitherto unexplored mass range. There has been a great deal of recent interest in the search for one such new particle, i.e., the charged Higgs boson [5],[6] of the two-Higgs-doublet version of the Standard Model [7]. In particular it was shown in [6] that for $m_t \simeq 150$ GeV a systematic comparison of the top signal in different decay channels provides an effective signature for charged Higgs bosons up to a mass of $m_H \simeq 100$ GeV at the Tevatron upgrade. For the theoretically most attractive two-Higgs-doublet model of MSSM (minimal supersymmetric Standard Model) one expects an observable signal throughout the allowed coupling parameter space. Thus one can probe the charged Higgs mass up to about 100 GeV unambiguously for this model. This is already larger than the charged Higgs discovery limit of 80-90 GeV at LEP-II [8],[9]. However, it is not large enough considering the theoretical expectation of $m_H > m_W$ in MSSM [7]. It should be mentioned here that, unlike the neutral Higgs mass, the charged Higgs mass is insensitive to the radiative correction from the heavy top quark, so that this tree-level bound remains valid for most of the parameter space [9].

In view of the above discussion it is important to devise means of extending the charged Higgs probe beyond 100 GeV without restricting ourselves to specific corners of the coupling parameter space. This is of course not possible at the Tevatron upgrade, where both the signal size and the signal/background ratio were seen to become marginal in the region of the coupling parameter $tan\ \beta \sim \sqrt{(m_t/m_b)}$ [6]. However, one expects a much larger size of the signal at LHC/SSC due to the larger $t\bar{t}$ cross-section and luminosity. For $m_H > 100$ GeV, the increasing gap between the charged Higgs and W boson masses offers the possibility of enhancing the signal/background ratio by suitable kinematic cuts. As we shall see in this note, it is possible to exploit the above two features to devise a viable charged Higgs signature which holds up to $m_H = m_t$ - 20 GeV and throughout the allowed coupling parameter space of MSSM. Thus it seems possible to probe for the charged Higgs mass to within 20 GeV of the top quark mass at these future hadron colliders, i.e., up to 130 GeV for $m_t \simeq 150$ GeV, going up to 180 GeV for $m_t \simeq 200$ GeV. This represents an important discovery limit, as it seems impossible to probe the region $m_H \geq m_t + m_b$ at hadron colliders [10].

The essential features of the two-Higgs-doublet model are as follows. It contains two $SU(2)$ doublets of complex scalar fields

$$\begin{pmatrix} \phi_1^0 \\ \phi_1^- \end{pmatrix} \begin{pmatrix} \phi_2^+ \\ \phi_2^0 \end{pmatrix}$$

with vacuum expectation values (v.e.v.s)

$$< \phi_1^0 >= v_1/\sqrt{2}, \quad < \phi_2^0 >= v_2/\sqrt{2} \tag{1}$$

which satisfy the W mass constraint

$$v_1^2 + v_2^2 = v^2, \quad (v = 246\ \text{GeV}) \tag{2}$$

This leaves one free parameter, i.e., the ratio of the two v.e.v.s

$$tan\beta = v_2/v_1 \tag{3}$$

After absorbing the three Goldstone bosons one is left with five physical states - the neutral scalars h^0, H^0 and pseudoscalar A^0 along with the charged states $H^\pm$. We shall be concerned only with the charged states, i.e.,

$$H^\pm = \phi_2^\pm \cos\beta - \phi_1^\pm \sin\beta \tag{4}$$

The two-Higgs-doublet model represents a minimal extension of the Standard Model which automatically satisfies the constraint of $\rho = 1$ at the tree level. Furthermore, the absence of flavour changing neutral current at the tree level can be naturally ensured via the Glashow-Weinberg theorem [11], which states that the tree-level FCNC mediated by Higgs bosons will be absent if all the fermions of the same electric charge have Yukawa couplings to only one Higgs doublet. A very important model automatically satisfying this constraint is the minimal supersymmetric extension of the Standard Model (MSSM), where the up-type quarks have Yukawa couplings to one Higgs doublet (ϕ_2, say) while the down-type quarks and charged leptons couple to the other. This model has received wide attention as it provides the most economical solution to the hierarchy problem of the Standard Model. Moreover, it offers the possibility of explaining the observed quark mass hierarchy $m_c \gg m_s$ and $m_t \gg m_b$ in terms of that of the v.e.v.s $v_2 \gg v_1$. In this model, the Yukawa couplings of the physical charged Higgs field of Eq. (4) to fermions are given by

$$\begin{aligned} \mathcal{L} = \frac{g}{\sqrt{2}m_W} H^+ \; \Big\{ & \; \cot\beta V_{ij}\; m_{ui}\bar{u}_i d_{jL} \\ & + \; tan\beta\; V_{ij} m_{dj}\bar{u}_i d_{jR} \\ & + \; tan\beta\; m_{\ell j}\bar{\nu}_j \ell_{jR} \; \Big\} + h.c. \end{aligned} \tag{5}$$

where V_{ij} are the KM matrix elements. One has identical charged Higgs couplings to the fermions in the E_6 superstring-inspired model [12] as well; but this model gives a less restrictive mass bound ($m_H > 53$ GeV) than the MSSM. We shall concentrate on the above coupling scheme of Eq. (5) in view of the wide theoretical interest behind the underlying models. Besides, as shown in Ref. [6], it is only for this coupling scheme that one can ensure an observable charged Higgs signal throughout the allowed range of the coupling parameter $tan\beta$. This range is summarized below [13].

The validity of perturbation theory implies upper bounds on the charged Higgs-fermion couplings appearing in Eq. (5). Requiring the tbH^+ coupling in the first term to be bounded by the strong coupling constant $4\pi\alpha_s (\simeq 1.5)$ gives a lower bound on $tan\beta$, i.e.,

$$tan\beta > m_t/600 \text{ GeV } (\simeq 1/4) \tag{6}$$

The size of this coupling can also be constrained by the charged Higgs exchange contributions to $B_d - \bar{B}_d$ mixing, $b \to s\gamma$ decay and CP violation in K decay [13]. They give a slightly better bound

$$tan\beta > 0.4 \tag{7}$$

for $m_t \sim 150$ GeV and $m_H \sim 100$ GeV. The perturbative limit on the tbH^+ coupling appearing in the second term of Eq. (5) gives the upper bound

$$tan\beta < 600 \text{ GeV}/m_b \; (\simeq 120) \tag{8}$$

Thus the region of interest in the coupling parameter space is

$$0.4 < tan\beta < 120 \tag{9}$$

While the lower bound holds for any two-Higgs-doublet model, the upper bound is specific to those where the up- and down-type quarks have Yukawa couplings to separate Higgs doublets like the MSSM [1]. It should be remarked here that we have adopted the most general definition of MSSM implying only the minimal particle content [7]. The most predictive form of this model, characterized by minimal set of SUSY breaking parameters at the grand unification point, leads to a more restrictive range of the coupling parameter [15]

$$1 < tan\beta < m_t/m_b \tag{10}$$

However, we shall consider the more general range of the coupling parameter space given by Eq. (9) above. In any case the most unfavourable region of this parameter space for the charged Higgs signal ($tan\beta \sim \sqrt{m_t/m_b}$) occurs in the middle of the range (10), as we shall see below.

The size of the charged Higgs signal vs. the W boson background in top quark decay is controlled by the relative decay widths of $t \to bH^+$ and $t \to bW^+$. In the diagonal KM matrix approximation one gets, from Eq. (5),

$$\Gamma_{t\to bH^+} = \frac{g^2}{64\pi m_W^2 m_t}\,\lambda^{1/2}(1, \frac{m_b^2}{m_t^2}, \frac{m_H^2}{m_t^2})\Big[(m_t^2\cot^2\beta + m_b^2 tan^2\beta)\,(m_t^2 + m_b^2 - m_H^2) + 4m_t^2 m_b^2\Big] \tag{11}$$

and the corresponding decay width into the W boson is

$$\Gamma_{t\to bW^+} = \frac{g^2}{64\pi m_W^2 m_t}\,\lambda^{1/2}(1, \frac{m_b^2}{m_t^2}, \frac{m_W^2}{m_t^2})\Big[m_W^2(m_t^2 + m_b^2) + (m_t^2 - m_b^2)^2 - 2m_W^4\Big] \tag{12}$$

Thus one gets the branching fraction

$$B(t \to bH^+) = \Gamma_{t\to bH^+}/(\Gamma_{t\to bH^+} + \Gamma_{t\to bW^+}) \tag{13}$$

From Eq. (5) one can also calculate the two significant charged Higgs decay widths, i.e.,

$$\Gamma_{H^+\to\tau^+\nu} = \frac{g^2 m_H}{32\pi m_W^2}\, m_\tau^2 tan^2\beta \tag{14}$$

$$\Gamma_{H^+\to c\bar{s}} = \frac{3g^2 m_H}{32\pi m_W^2}\,(m_c^2\cot^2\beta + m_s^2 tan^2\beta) \tag{15}$$

and the branching fraction

$$B(H^+ \to \tau^+\nu) = m_\tau^2 tan^2\beta/3(m_c^2\cot^2\beta + m_s^2 tan^2\beta) + m_\tau^2 tan^2\beta \tag{16}$$

The effect of the QCD correction has been analyzed in detail in the second paper of Ref. [6] following the formalism of Ref. [16]. The most significant effect comes from the $H^+ \to c\bar{s}$ decay width. In the leading log approximation the QCD correction can be simply implemented by replacing the quark mass terms appearing in the width of Eq. (15), or equivalently in the Yukawa couplings of Eq. (5), by the running mass

$$\tilde{m}_q(m_H) = m_q\,\left(\frac{\ln(2m_q/\Lambda)}{\ln(m_H/\Lambda)}\right)^{\frac{12}{33-2N_f}} \tag{17}$$

where one has assumed the standard initial condition [16]

$$\tilde{m}_q(2m_q) = m_q \tag{18}$$

[1] There are no more constraints on this parameter from the LEP data once the radiative corrections are taken into account [14].

The initial values are chosen to be $m_c = 1.5$ GeV and $m_s = 0.2$ GeV. The quantity of phenomenological interest is of course the resulting branching fraction of Eq. (16), which is clearly insensitive to m_s.

The corresponding branching fractions for W decay are of course given by the universality of W coupling to leptons and quarks, i.e., 10 % into each lepton pair and 70 % into hadrons (including the small QCD enhancement of hadronic width by ~ 4 %). The striking difference between the two sets of branching fractions makes it possible to separate the charged Higgs and W contributions by comparing the relative size of the $t\bar{t}$ signal in different decay channels [6]. Like W, the charged Higgs has also to be identified through its leptonic (i.e., tau) decay to avoid the large QCD background. Thus it is the product of the two branching fractions (13) and (16) that controls the size of the charged Higgs signal.

These two branching fractions are shown in Fig. 1 against the coupling parameter $tan\beta$. The branching fraction for charged Higgs production $t \rightarrow bH$ is shown for $m_t = 150$ GeV ($m_H = 110$, 130 GeV) and $m_t = 200$ GeV ($m_H = 160$, 180 GeV), while the $H \rightarrow \tau\nu$ decay branching fraction is practically independent of m_H. The $t \rightarrow bH$ branching fraction becomes very small around $tan\beta \sim (m_t/m_b)^{1/2} \sim 6$ where Eq. (11) has a minimum. This is partly compensated by the maximal value of the $H \rightarrow \tau\nu$ branching fraction in this region. As remarked in Ref. [6], this compensation mechanism is typical of the coupling scheme of Eq. (5) and ensures a viable charged Higgs signal throughout the allowed $tan\beta$ space in this scheme for $m_H \sim m_W$. However, the compensation is no longer adequate as $m_H \rightarrow m_t$. For instance, in the extreme case of $m_t = 200$ GeV ($m_H = 180$ GeV) one sees that the signal/background ratio for the τ channel is only ~ 2 % around $tan\beta \simeq 6$. For the 2τ channel, corresponding to τ-decay of both t and $\bar{t}$, one gains a combinatorial factor of 2 raising this ratio to ~ 4 %. Thus one needs a background rejection factor of ~ 25 from kinematic cuts to have a viable charged Higgs signal in this region. We shall see below that it is indeed possible to devise such kinematic cuts and ensure a signal/background ratio $\gtrsim 1$ as well as a sizeable signal throughout the allowed $tan\beta$ space.

The charged Higgs signal and the W boson background are estimated using a parton level event generator program. The basic process of interest is $t\bar{t}$ production through gluon-gluon or quark-antiquark fusion followed by their decay into charged Higgs or W boson channels ($t \rightarrow bH, bW$), i.e.,

$$gg \text{ or } q\bar{q} \rightarrow t\bar{t} \rightarrow b\bar{b}(H^+H^-, H^\pm W^\mp, W^+W^-) \tag{19}$$

Here the first two terms in the parentheses represent the charged Higgs signal and the third one the W background. This is followed by the charged boson decays

$$H \rightarrow \tau\nu \tag{20a}$$

$$H \rightarrow c\bar{s} \tag{20b}$$

with the branching fractions of Eq. (16), and

$$W \overset{10\%}{\longrightarrow} e\nu, \mu\nu, \tau\nu \tag{21a}$$

$$W \overset{70\%}{\longrightarrow} q\bar{q}' \tag{21b}$$

Finally, the τ is to be observed in its muonic or hadronic decay channel

$$\tau \overset{18\%}{\longrightarrow} \nu_\tau \nu_\mu \mu \tag{22a}$$

$$\tau \overset{64\%}{\longrightarrow} \nu_\tau\, q\bar{q}' \tag{22b}$$

as a soft muon or a narrow jet (τ-jet), accompanied by a significant amount of missing p_T. We shall largely concentrate on the hadronic decay channel of τ and refer to it simply as the τ-channel.

The $t\bar{t}$ signal in the hard dilepton channel

$$t\bar{t} \to b\bar{b}W^+W^- \to b\bar{b}\ell^+\bar{\nu}\ell^-\nu, \quad (\ell = e, \mu) \tag{23}$$

(with $p_\ell^T > 20$ GeV, say) can be used to normalize the W^+W^- contribution since the charged Higgs does not contribute to this channel. Then the W^+W^- background in any other channel is predicted by universality [Eqs. (21),(22)]. A sizeable excess over this prediction will constitute a charged Higgs signal, whose magnitude is also predicted by Eqs. (13) and (14). Thus the uncertainties associated with the $t\bar{t}$ production are effectively factored out. One can see from Fig. 1 that the predicted W^+W^- contribution to any channel would depend on m_H and $tan\beta$; the maximal value obtained at $tan\beta \simeq 6$ corresponds to the Standard Model prediction (see Figs. 3 and 4). However, this dependence drops out when normalized with respect to the hard dilepton channel [2].

The results presented below are obtained using the structure functions and α_s of Ref. [16]. We have also cross-checked them by using the corresponding QCD parameters of Ref. [17]. There is essentially no difference apart from a drop of overall normalization by a factor of ~ 2, mainly due to α_s. The normalization has of course no effect on the relative size of the signal in different channels as mentioned above. For the same reason one expects the result to be insensitive to higher-order QCD corrections. We concentrate below on the most viable channels for the charged Higgs signal and the LHC energy of $\sqrt{s} = 16$ TeV.

<u>2τ channel</u>
It corresponds to τ decay of both the charged bosons of (19) followed by hadronic decay of τ (22b). We have chosen a minimal set of cuts

$$p^T_{\tau-jet} > 10 \text{ GeV}, \quad p^T_{miss} > 20 \text{ GeV} \tag{24}$$

which come by default. Similarly we have chosen a minimal isolation cut of accompanying $p_T < 5$ GeV within 0.4 rad of the τ direction. They can be increased significantly without a serious reduction in cross-section [3]. This channel offers the best signal/background ratio because (i) the signal gets contributions from both HH and HW terms and (ii) the latter is enhanced by a combinatorial factor of 2. The disadvantage is that it is not possible to reconstruct the charged boson masses because of the large number of neutrinos. Nonetheless one can separate the signal from the background by exploiting the fact that as $m_H \to m_t$ the accompanying b-jet becomes soft. Thus the WW background of (19) has two hard accompanying jets while the signal has at least one soft jet.

Figure 2a shows the p^T distribution of the hardest accompanying jet for the signal and background events for the most unfavourable coupling parameter $tan\beta = 6$. For this choice the signal is dominated by the HW term and consequently the peak value of the accompanying p^T_{j1} is not very different from the WW background. Note, however, that, in the region $p^T_{j1} < 30$ GeV, the background is doubly suppressed by the probability of each accompanying jet becoming soft, while the signal is suppressed singly. Thus one can get a signal/background ratio $\simeq 1$ by

[2]The observation of a $t\bar{t}$ signal in the hard dilepton channel below the level of standard model prediction is in principle indicative of a charged Higgs boson. But it cannot be used in practice because of the uncertainty in the production cross-section.

[3]The 2τ background from Drell-Yan and Z decay can be readily distinguished by its azimuthally back-to-back configuration and no missing p_T normal to this 2τ axis.

ensuring that there is no accompanying b-jet with $p^T > 30$ GeV[4]. Figure 3a shows the resulting signal and background over the allowed range of $tan\beta$ at the LHC energy. It shows a viable signal up to $m_H \simeq m_t$ - 20 GeV with a signal/background ratio $\gtrsim 1$ and a signal size $\gtrsim 10$ fb. The latter corresponds to a minimum of 100(1000) events for an annual luminosity of 10(100) fb^{-1}.

Figure 2b shows the p^T distribution of the second hardest b-jet for the signal and background for $tan\beta = 6$. Although the background peaks at a significantly higher value of p^T_{j2} compared to the signal, there is a residual background left in the $p^T_{j2} = 0$ region. This is due to the jet folding algorithm which merges the b-jets emerging within an opening angle of 1/2 radian into one. This limits the background suppression potential of a low p^T_{j2} cut. Figure 3b shows the signal and background over the allowed $tan\beta$ range with $p^T_{j2} < 20$ GeV. The lower set of curves is evaluated with $10 < p^T_{j2} < 20$ GeV to avoid the residual background at $p^T_{j2} = 0$. Comparing Figs. 3a and 3b, we see that the cut on the hardest jet corresponds to a smaller signal size but better signal/background ratio. Besides it seems to us simpler to implement experimentally.

τ + hard μ channel

It corresponds to τ decay of one of the charged bosons of (19) and muonic decay of the other. Thus the signal comes only from the HW term and moreover loses the advantage of the combinatorial factor of 2 vs. the WW background. We choose a minimal set of cuts

$$p^T_{\tau-jet} > 10 \text{ GeV}, \quad p^T_{miss} > 20 \text{ GeV}, \quad p^T_{\mu} > 20 \text{ GeV} \tag{25}$$

which have little effect on the cross-section. Supplementing this with the $p^T_{j1} < 30$ GeV cut, we get the signal and background curves shown in Fig. 4a.

While the signal size remains viable through the allowed $tan\beta$ range, the signal/background ratio falls significantly below 1 in the neighbourhood of $tan\beta \simeq 6$.

τ + soft μ channel

It corresponds to τ decay of both the charged bosons of (19) followed by the muonic decay of one τ (22a). The smaller muonic branching fraction of τ results in a smaller signal size compared to the 2τ channel. Besides one has to include the soft μ tail from the direct $W \to \mu$ decay, which makes the signal/background ratio somewhat smaller as well. The cuts used are

$$p^T_{\tau-jet} > 10 \text{ GeV}, \quad p^T_{miss} > 20 \text{ GeV}, \quad p^T_{\mu} = 5 - 20 \text{ GeV} \tag{26}$$

where the p^T_{μ} cut is optimized to retain most the τ-decay muons ($\sim$ 50 %) while minimizing contamination from direct W decay ($\sim$ 10 %). Supplementing this with the $p^T_{j1} < 30$ GeV cut, we get the signal and background shown in Fig. 4b. Compared to the 2τ channel of Fig. 3a, one sees a smaller signal size and signal-to-background ratio. Nonetheless it could be viable for charged Higgs search up to $m_H = m_t$ - 20 GeV with the high luminosity option of LHC (= 100 fb^{-1}).

τ + multijet channel

It corresponds to τ decay of one of the charged bosons of (19) and hadronic decay of the other. For $tan\beta > 1$, the signal/background ratio is identical to the τ + hard μ channel, while the signal size is a factor of 7 higher [Eq. (21)]. The minimal cuts are

$$p^T_{\tau-jet} > 10 \text{ GeV}, \quad p^T_{miss} > 20 \text{ GeV}, \quad n_j \geq 2, \quad p^T_{j1,2} > 40 \text{ GeV} \tag{27}$$

[4]Identification of the b-jet is not necessary, since one expects only a tiny fraction of $t\bar{t}$ events to be accompanied by a QCD jet of $p^T > 30$ GeV [18]. Thus it is sufficient to ensure that there are no accompanying jets of $p^T > 30$ GeV.

The disadvantage of this channel, unlike the previous ones, is a significant background from W + QCD jets even after the large $p^T_{j1,2}$ cut. The advantage is the absence of neutrinos in the decay of one of the two charged bosons. Thus one can reconstruct the $W(H)$ mass from, e.g., the transverse mass of the τ-jet and missing-p_T system. Figure 6 shows this transverse mass distribution of the WH signal and the WW background for the most unfavourable value of $tan\beta = 6$. The background gets kinematically cut off at the W boson mass. Although the effect of resolution smearing is not shown, one can check that with a $\Delta M_{tr} = 10$ GeV, less than 1 % of the background spills over to the $M_{tr} > 100$ GeV region. This would ensure a signal/background ratio $\gtrsim 1$. With good b-jet identification one could also use the $p^T < 30$ GeV cut on the b-jets for suppressing the WW background. On the other hand one may need an identified large p_T b-jet to control the background from W+ QCD jets. Therefore, we have not explored this possibility further. It is clear from Fig. 5, however, that the τ + multijet channel can give significant clues about the charged Higgs mass from the tail of the M_{tr} distribution. It is therefore an important channel for the charged Higgs search, provided one can identify τ in a multijet environment.

It is evident from the above analysis that good τ-jet identification is crucial to charged Higgs search via top quark decay at hadron colliders. We have not assumed, however, measurement of τ charge or polarization. If polarization measurement is available, then one can also use the correlation between the τ charge and polarization to separate the charged Higgs signal from the W boson background as recently discussed in Ref. [19], since one expects $\tau^-_L(\tau^+_R)$ from $W \to \tau\nu$ and $\tau^-_R(\tau^+_L)$ from $H \to \tau\nu$. Of course the polarization measurement may not reach the 2 % accuracy required to probe through the full parameter space by itself. However, once the sample of τ events have been enriched by, e.g., the $p^T_{j1} < 30$ GeV cut, one needs no more than 20 % accuracy in the polarization measurement to confirm the charged Higgs signal. A quantitative analysis of this polarization effect is in progress.

In summary, we have tried to explore the prospect of charged Higgs search via top quark decay at LHC/SSC and identify the most effective channel and kinematic cut for this purpose. They are the 2τ channel and a p_T cut on the accompanying b-quark jets. They provide a sizeable charged Higgs signal and a signal/background ratio $\gtrsim 1$ up to $m_H \simeq m_t$ - 20 GeV, which hold throughout the allowed range of coupling parameters in the MSSM. The calculations are done for LHC energy; but of course what is true for LHC is even more true for SSC. Thus for the MSSM the charged Higgs mass can be unambiguously explored to within 20 GeV of the top quark mass - i.e., up to 130 GeV for $m_t \simeq 150$ GeV, going up to 180 GeV for $m_t \simeq 200$ GeV. This means that a relatively heavy top may be bad news for the top quark search but a good one for the charged Higgs boson.

It is a pleasure to thank Drs. G. Altarelli, H. Haber, B. Grzadkowski, Z. Kunszt and F. Zwirner for discussions and R.M. Godbole for drawing my attention to Ref. [19].

References

[1] CDF Collaboration: F. Abe et al., *Phys.Rev.Lett.* **64** (1990) 142;
A. Barbaro-Galtieri, Fermilab Conf-91/66-E (to be published in the proceedings of the 1990 Summer Study on High Energy Physics, Snowmass, Colorado).

[2] G. Altarelli and P. Franzini, *Z.Phys.* **C39** (1988) 271;
P. Franzini, *Physics Reports* **173** (1989) 1 and references therein.

[3] See, e.g.: J. Ellis and G.L. Fogli, *Phys.Lett.* **B232** (1989) 139;
P. Langacker, *Phys.Rev.Lett.* **63** (1989) 1920;
J. Steinberg, *Physics Reports* **203** (1991) 345.

[4] S. Gupta and D.P. Roy, *Z.Phys.* **C39** (1988) 417;
H. Baer, V. Barger and R.J.N. Phillips, *Phys.Rev.* **D39** (1989) 3310;
F. Cavanna, D. Denegri and T. Rodrigo, Proceedings of ECFA-LHC Workshop, Vol. II, p. 329, CERN 90-10 (1990).

[5] V. Barger and R.J.N. Phillips, *Phys.Rev.* **D41** (1990) 884;
A.C. Bawa, C.S. Kim and A.D. Martin, *Z.Phys.* **C47** (1990) 75;
M. Felcini, Proceedings of ECFA-LHC Workshop, Vol. II, p. 414, CERN 90-10 (1990);
R.M. Barnett et al., Proceedings of 1990 Summer Study on High Energy Physics, Snowmass, Colorado (to be published).

[6] R.M. Godbole and D.P. Roy, *Phys.Rev.* **D43** (1991) 3640;
M. Drees and D.P. Roy, *Phys.Lett.* **B269** (1991) 155.

[7] For a review of Higgs physics, see, e.g.:
J.F. Gunion, H.E. Haber, G. Kane and S. Dawson, the Higgs Hunters' Guide, Addison Wesley, Reading, MA (1990);
H.E. Haber, in Phenomenology of the Standard Model and Beyond, eds. D.P. Roy and P. Roy, World Scientific (1990), p. 197.

[8] S. Komamiya, *Phys.Rev.* **D38** (1988) 2158.

[9] A. Brignole, J. Ellis, G. Ridolfi and F. Zwirner, CERN Preprint TH. 6151/91 (1991).

[10] J.F. Gunion et al., Proceedings of 1987 Berkeley Workshop on Experiments, Detectors and Experimental Areas of the Supercollider, eds. P. Donaldson and M. Gilchriese, World Scientific (1988), p. 110.

[11] S. Glashow and S. Weinberg, *Phys.Rev.* **D15** (1977) 1958;
E.A. Paschos, *Phys.Rev.* **D15** (1977) 1966;
K. Kang and J. Kim, *Phys.Lett.* **64B** (1976) 93.

[12] J.L. Hewett and T.L. Rizzo, *Physics Reports* **183** (1989) 193.

[13] V. Barger et al., *Phys.Rev.* **D41** (1990) 3421;
A. Buras et al., *Nucl.Phys.* **B337** (1990) 284;
J.F. Gunion and B. Grzadkowski, *Phys.Lett.* **B243** (1990) 301.

[14] J. Ellis, G. Ridolfi and F. Zwirner, *Phys.Lett.* **B257** (1991) 83;
H.E. Haber and R. Hempfling, *Phys.Rev.Lett.* **66** (1991) 1815;
ALEPH Collaboration, D. Decamp et al., *Phys.Lett.* **B165** (1991) 475.

[15] G. Ridolfi, G.G. Ross and F. Zwirner, Proceedings of ECFA-LHC Workshop, Vol. II, p. 608, CERN 90-10 (1990).

[16] M. Gluck, F. Hoffman and E. Reya, *Z.Phys.* **C13** (1982) 119.

[17] J. Kwiecinski, A.D. Martin, R.G. Roberts and W.J. Stirling, *Phys.Rev.* **D42** (1990) 3645. This set of structure functions was accessed via "The Structure Function Package", H. Plothow-Besch, Proceedings of 3rd Workshop on Detector and Event Simulation in High Energy Physics, Amsterdam, 8-12 April 1991.

[18] M.L. Mangano, P. Nason and G. Ridolfi, Pisa Preprint UPRF/91/308 (1991).

[19] B.K. Bullock, K. Hagiwara and A.D. Martin, Durham Preprint DTP/91/42 (1991).

FIGURE CAPTIONS

Figure 1 Branching fractions for $t \to bH$ for $m_t = 150$ GeV with $m_H = 110$ and 130 GeV (solid upper and lower lines), and $m_t = 200$ GeV with $m_H = 160$ and 180 GeV (dashed upper and lower lines). The branching fraction of charged Higgs decay into τ lepton is shown by the dotted line. The allowed range of $tan\beta(\gtrsim 0.4)$ is indicated by the hatched line.

Figure 2 The distribution of 2τ events in the transverse momentum of the accompanying b-jets: a) hardest jet and b) second hardest jet. The normalizations of the charged Higgs signal (solid lines) and the WW background (dashed lines) correspond to the most unfavourable value of $tan\beta$ (= 6). The upper and lower sets of curves correspond to $m_t = 150$ GeV ($m_H = 110$, 130 GeV) and $m_t = 200$ GeV ($m_H = 160$, 180 GeV) respectively in this and the following figures. The energy is the LHC energy of $\sqrt{s} = 16$ TeV.

Figure 3 a) The charged Higgs signal (solid line) and WW background (dotted line) for the 2τ channel with a $p^T < 30$ GeV cut on the hardest accompanying jet. In each set of curves the lower solid (upper dashed) lines correspond to the higher Higgs mass.
b) Same as above with a $p^T < 20$ GeV cut on the second hardest jet ($10 < p^T_{j2} < 20$ GeV for the lower set of curves).

Figure 4 The charged Higgs signal (solid line) and WW background (dotted line) for
a) $\tau+$ hard $\mu(p^T > 20$ GeV) channel and
b) $\tau+$ soft $\mu(p^T_\mu = 5$-20 GeV) channel.
In each case there is a $p^T < 30$ GeV cut on the hardest accompanying jet.

Figure 5 The distribution of the τ + multijet events in the transverse mass of the τ-jet and the missing p_T system. The normalization of the charged Higgs signal (solid lines) and the WW background (dashed lines) shown corresponds to the most unfavourable value of $tan\beta = 6$.

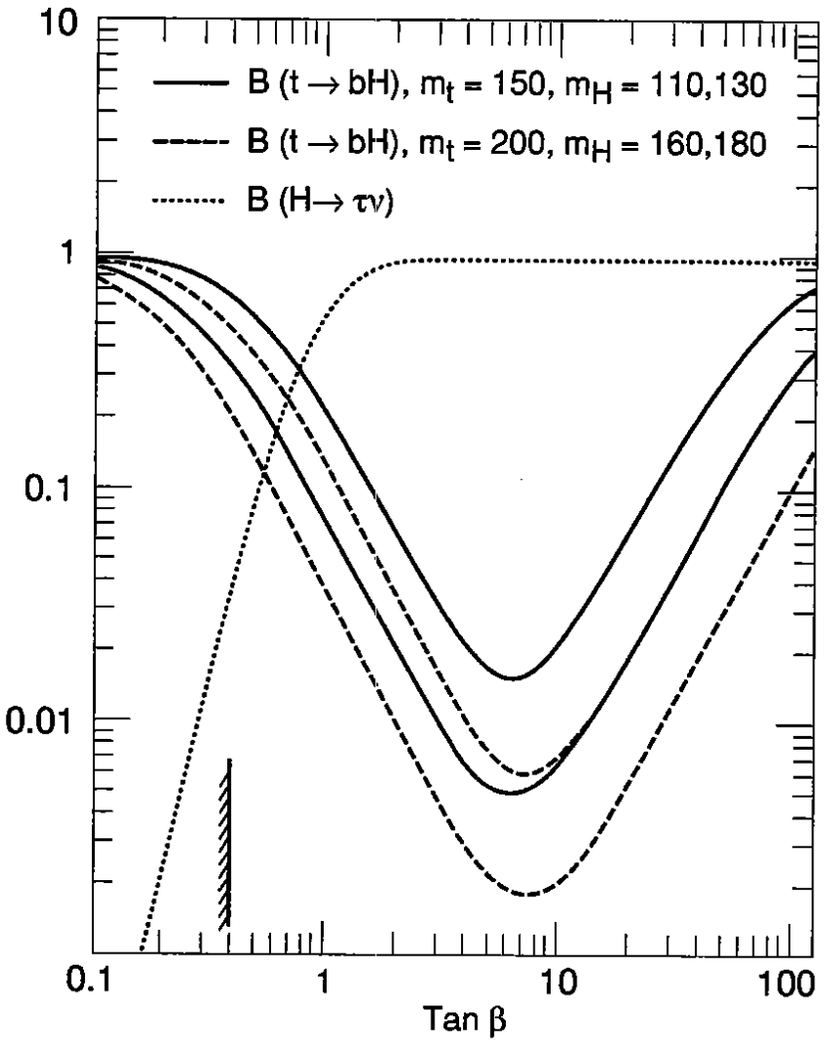
10
1
0.1
0.01
0.1
1
10
100
Tan β
B (t → bH), m_t = 150, m_H = 110,130
B (t → bH), m_t = 200, m_H = 160,180
B (H→ τν)

Fig. 1

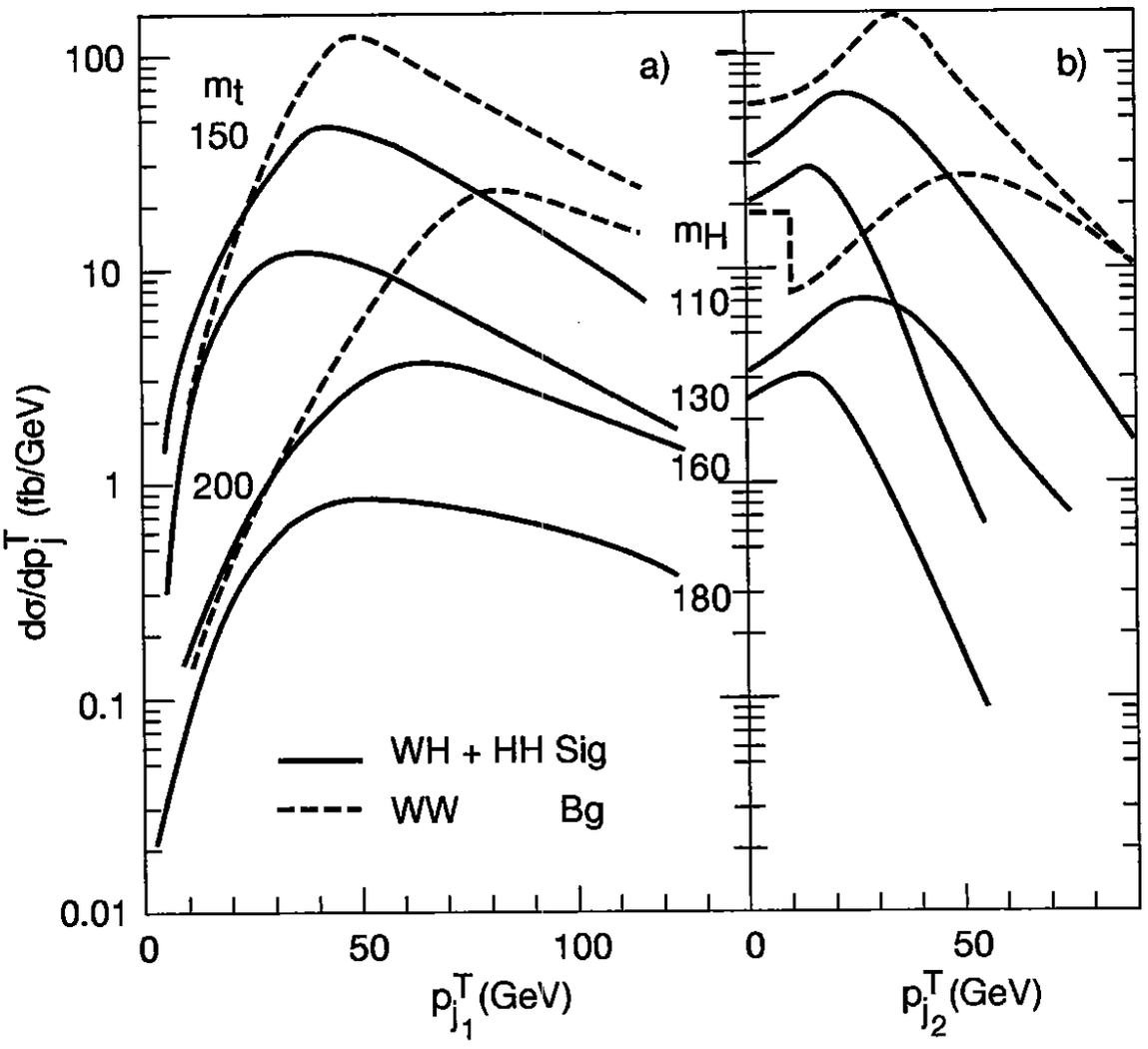
100
10
1
0.1
0.01
$d\sigma/dp_j^T$ (fb/GeV)
m_t
150
200
a)
b)
m_H
110
130
160
180
WH + HH Sig
WW Bg
0
50
100
$p_{j_1}^T$ (GeV)
0
50
$p_{j_2}^T$ (GeV)

Fig. 2

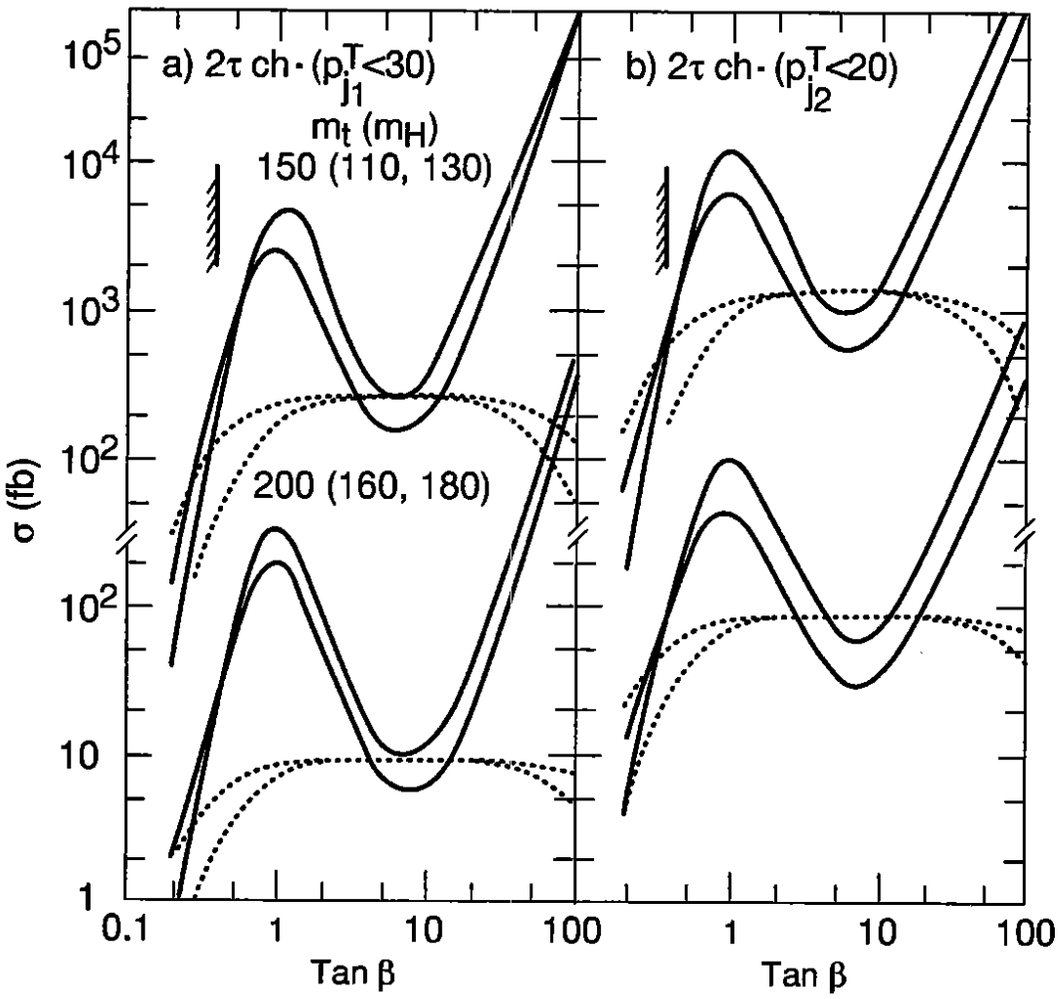
a) 2τ ch - (p_{j1}^T<30)
b) 2τ ch - (p_{j2}^T<20)
m_t (m_H)
150 (110, 130)
200 (160, 180)
σ (fb)
Tan β
Tan β

Fig. 3

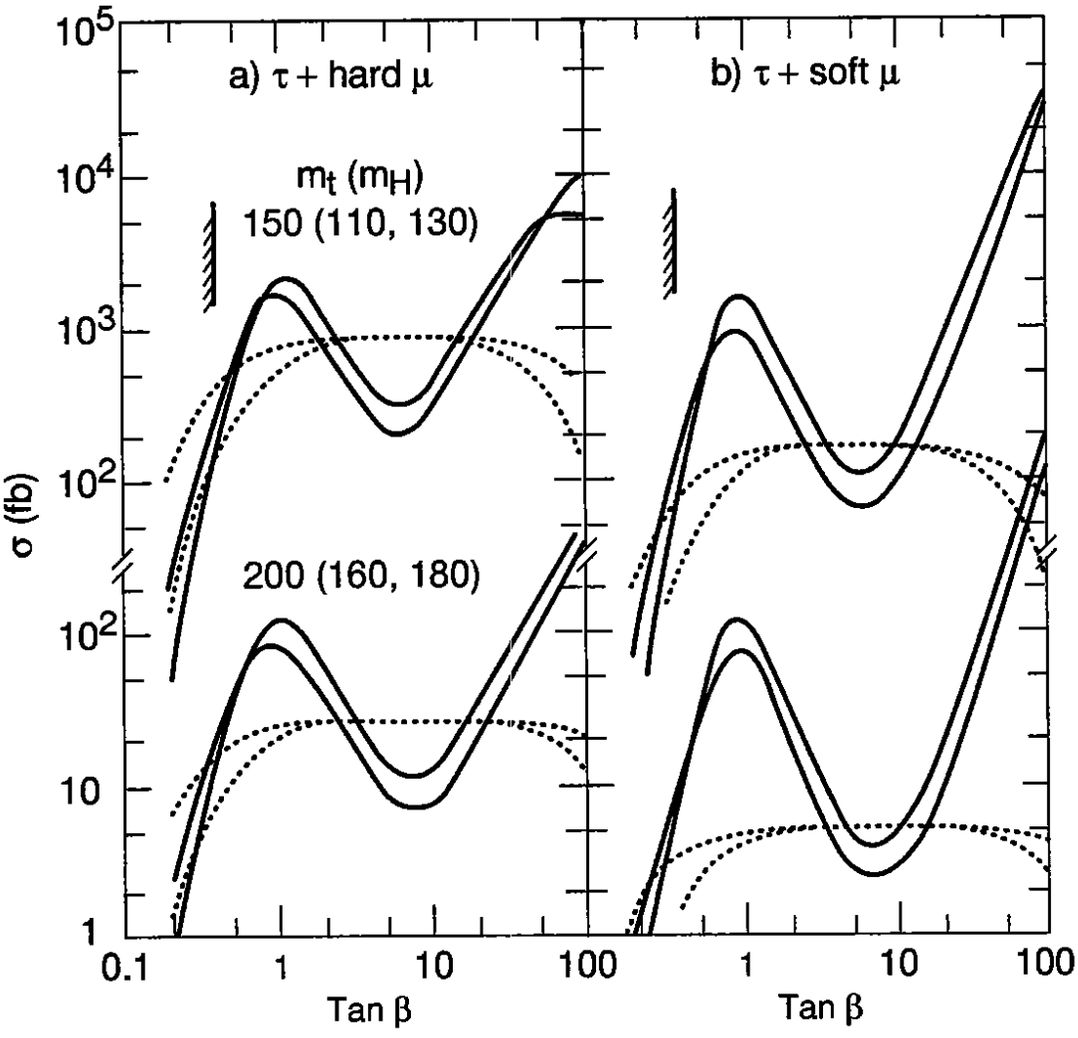

Fig. 4

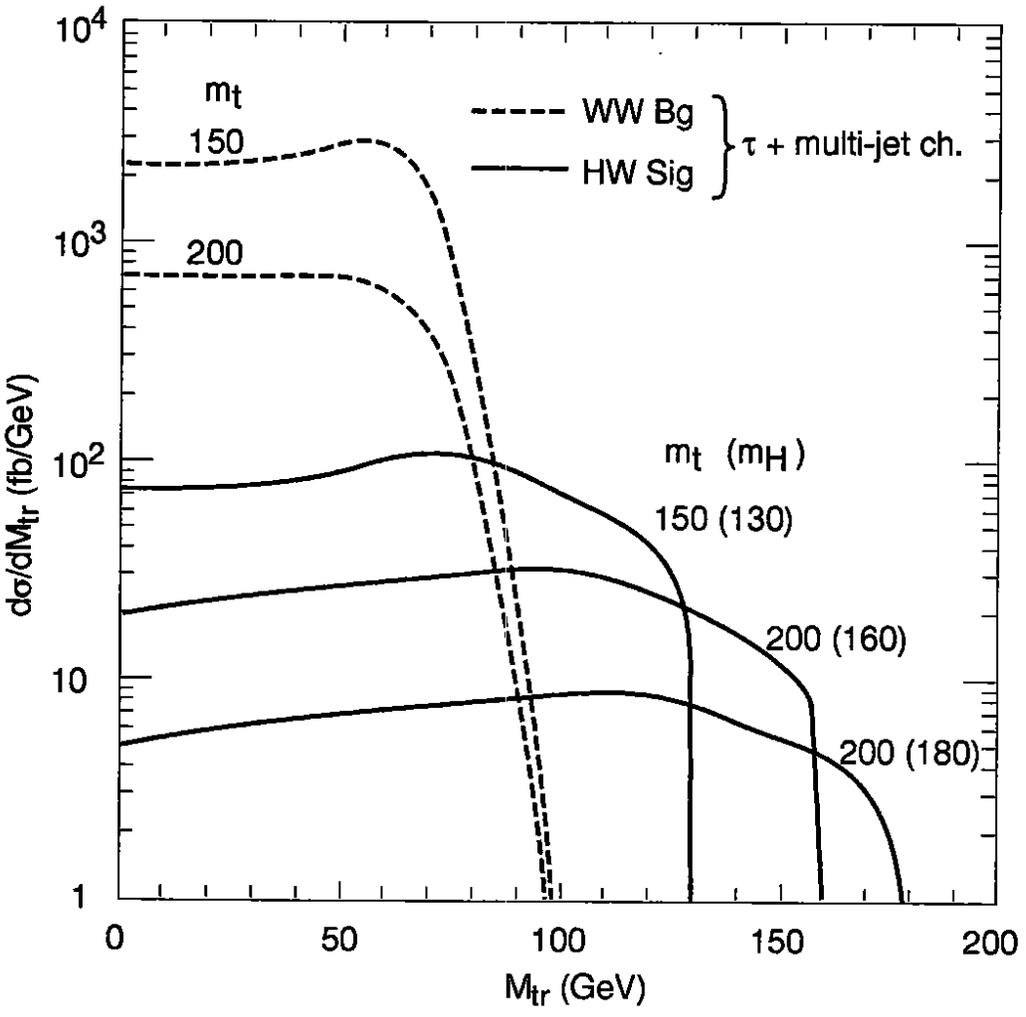
10^4
10^3
10^2
10
1
$d\sigma/dM_{tr}$ (fb/GeV)
m_t
150
200
WW Bg
HW Sig
τ + multi-jet ch.
m_t (m_H)
150 (130)
200 (160)
200 (180)
0
50
100
150
200
M_{tr} (GeV)

Fig. 5